OPEN ACCESS
IOP Publishing
Semiconductor Science and Technology
Semicond. Sci. Technol. **32** (2017) 024001 (7pp)
doi:10.1088/1361-6641/32/2/024001

Imaging electron motion in graphene

Sagar Bhandari[1] **and Robert M Westervelt**[1,2]

[1] School of Engineering and Applied Sciences, Harvard University, Cambridge, MA 02138, USA
[2] Department of Physics, Harvard University, Cambridge, MA 02138, USA

E-mail: sbhandar@fas.harvard.edu

Received 30 June 2016, revised 19 September 2016
Accepted for publication 10 November 2016
Published 5 January 2017

Abstract

A cooled scanning probe microscope (SPM) is an ideal tool to image electronic motion in graphene: the SPM tip acts as a scanning gate, which interacts with the electron gas below. We introduce the technique using our group's previous work on imaging electron flow from a quantum point contact in a GaAs 2DEG and tuning an InAs quantum dot in an InAs/InP nanowire. Carriers in graphene have very different characteristics: electrons and holes travel at a constant speed with no bandgap, and they pass through potential barriers via Klein tunneling. In this paper, we review the extension of SPM imaging techniques to graphene. We image the cyclotron orbits passing between two narrow contacts in a single-atomic-layer graphene device in a perpendicular magnetic field. Magnetic focusing produces a peak in transmission between the contacts when the cyclotron diameter is equal to the contact spacing. The charged SPM tip deflects electrons passing from one contact to the other, changing the transmission when it interrupts the flow. By displaying the change in transmission as the tip is raster scanned above the sample, an image of flow is obtained. In addition, we have developed a complementary technique to image electronic charge using a cooled scanning capacitance microscope (SCM) that uses a sensitive charge preamplifier near the SPM tip to achieve a charge noise level $0.13\ e\ Hz^{-1/2}$ with high spatial resolution 100 nm. The cooled SPM and SCM can be used to probe the motion of electrons on the nanoscale in graphene devices.

Keywords: graphene, electron motion, scanning probe, magnetic focusing, scanning capacitance, imaging

Introduction

A cooled scanning probe microscope (SPM) has been proven to be a powerful tool to image electron motion in a two-dimensional electron gas (2DEG) inside a GaAs/AlGaAs heterostructure [1–14]. Quantum hall edge states were imaged using a scanning single electron transistor (SET) as a charge sensor [6]. By using the capacitively coupled SPM tip to deflect electron trajectories, coherent electron flow from a quantum point contact (QPC) was imaged by displaying the change in conduction as the tip was raster scanned above the sample [7–14]. In addition, magnetic focusing of electrons in a GaAs 2DEG was imaged using this technique [13, 14]. A charged SPM tip can also be used to capacitively tune a quantum dot by displaying the dot conductance as the tip is raster scanned above, creating a bullseye pattern, in which the rings of high conductance correspond to Coulomb-blockade conductance peaks [15–19]. This approach has been applied to quantum dots formed in a GaAs 2DEG by surface gates [15], and to InAs quantum dots in an InAs/InP nanowire heterostructure [16–18]. Quantum dots in single-walled carbon nanotubes have been imaged using scanning force microscopy [20, 21].

The SPM has been proven to be a valuable tool to shed light on the physics of electron motion in graphene. Electron hole puddles in graphene were imaged using a scanning SET [22] and STM techniques [23]. Using a capacitively coupled SPM tip, universal conductance fluctuations in graphene were spatially mapped in graphene [24, 25]. Quantum dots in graphene nanostructures were imaged to reveal Coulomb-blockade conductance rings [26].

A wealth of 2D materials have been discovered in recent years that have exotic electronic properties [27]. Electrons in

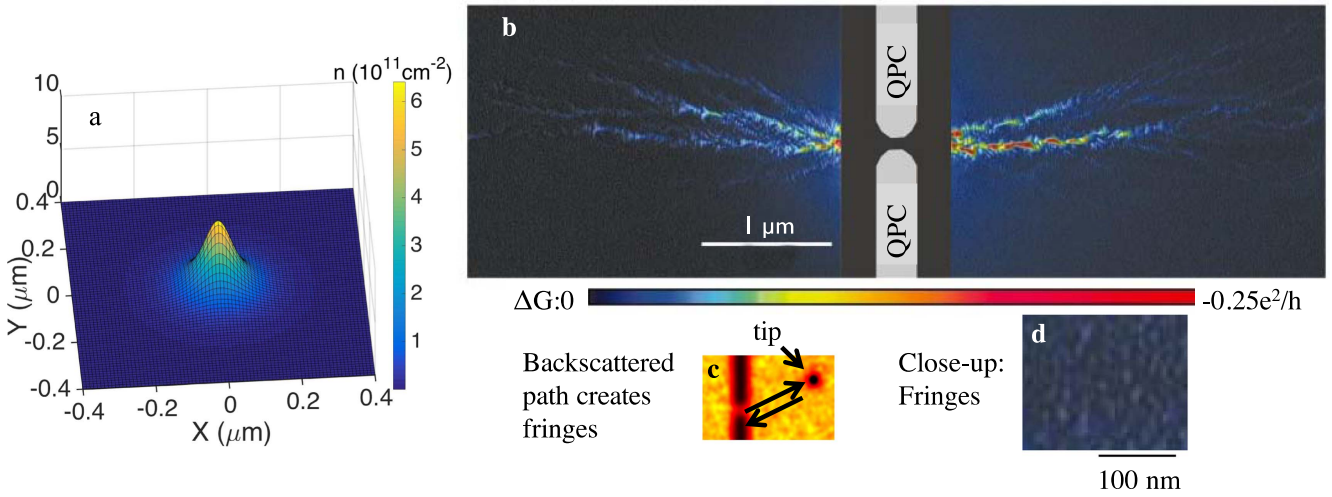

Figure 1. (a) Image charge density profile created by a charged SPM tip above the sample surface. The tip voltage depletes a small divot in the electron gas that scatters electron waves back to the QPC, reducing its conductance, as shown in the inset. By displaying the QPC conductance as the tip is raster scanned across the sample, an image of the electron flow is obtained. (b) Scanning probe microscopy images at temperature 4.2 K of electron flow from a quantum point contact. Branches in flow are created by small angle scattering from Si donor ions. The images reveal interference fringes spaced by half the Fermi wavelength, shown in the inset [7].

graphene have energies that increase linearly with their momentum at low energies. They are massless, chiral, Dirac fermions described by the Dirac equation [28] that display new phenomena, including the Anomalous quantum Hall effect, Klein tunneling, and Berry's phase [29–37]. Because graphene is a two-dimensional material with its surface completely exposed to the environment, the interface to the substrate plays an important role. Graphene devices on a silicon substrate typically have a mobility $\sim$10 000 cm^2 V^{-1} s^{-1}. Freely suspending graphene improves the mobility to $\sim$200 000 cm^2 V^{-1} s^{-1}, but limits the device architecture and functionality. Encasing the graphene in two hexagonal boron nitride (hBN) layers enhances the mobility to comparable values [38–40]. As a result, electrons can travel several microns without scattering at low temperatures and follow classical trajectories as their motion becomes ballistic.

In this paper, we review the extension of our previously developed SPM techniques [7–17] to image electron flow in graphene. A cooled SPM was used to image the circular cyclotron orbits of electrons at 4.2 K in a hBN/graphene/hBN device in an external magnetic field, directly showing ballistic transport [41, 42].

SPM imaging technique

Scanning gate microscopy uses a nanoscale tip as a local probe to image electron flow inside materials. In a scanning gate measurement, the trajectories of electrons can be mapped at low temperatures by having a conducting tip deflect electrons while the resulting change conductance is measured. A charge on the tip creates an image charge and a corresponding density change in the 2DEG below, shown by simulations in figure 1(a). Scattering by the dip in density below the tip deflects electron paths and changes the conductance of the sample. A map of the conductance versus tip position reveals the electronic trajectories in the sample.

Using this technique, we previously imaged the coherent flow of electron waves through a 2DEG from a QPC in GaAs/AlGaAs heterostructure [7]. Figure 1(b) shows an image of electron flow recorded using a scanning gate microscope, which includes dramatic branches caused by the focusing of electron paths by small angle scattering from charged donor impurities. As shown in figure 1(c), the tip voltage depletes a small divot in the electron gas below that scatters electron waves back through the QPC, reducing its conductance. By displaying the QPC conductance as the tip is raster scanned across the sample, an image of electron flow is obtained. The images shown in figure 1(d) revealed fringes corresponding to the interference of electron waves. The fringes were spaced at half a Fermi wavelength confirming the existence of coherent waves of electrons in 2DEG.

In addition, we have used a conducting SPM tip to tune a quantum dot [15–18]. Figure 2(a) shows the scanning gate setup to image electrons confined in quantum dots in a nanowire heterostructure [17]. The tip is scanned at a constant height above the nanowire while measuring the conductance through the device. The quantum dot is formed in a InAs/InP heterostructure by two InP barriers, as shown in figure 2(b). The number of electrons on the quantum dot is tuned by the capacitance between the tip and the dot and the tip voltage. As the tip is raster scanned above the dot at constant tip voltage, a display of the dot conductance versus tip position shows a bullseye pattern of Coulomb blockade peaks, where the number of electrons changes by one. Figure 2(c) shows the first electron added to the dot, confirmed by the fact that a regular series of Coulomb blockade peaks were observed at higher electron numbers, but none below [17].

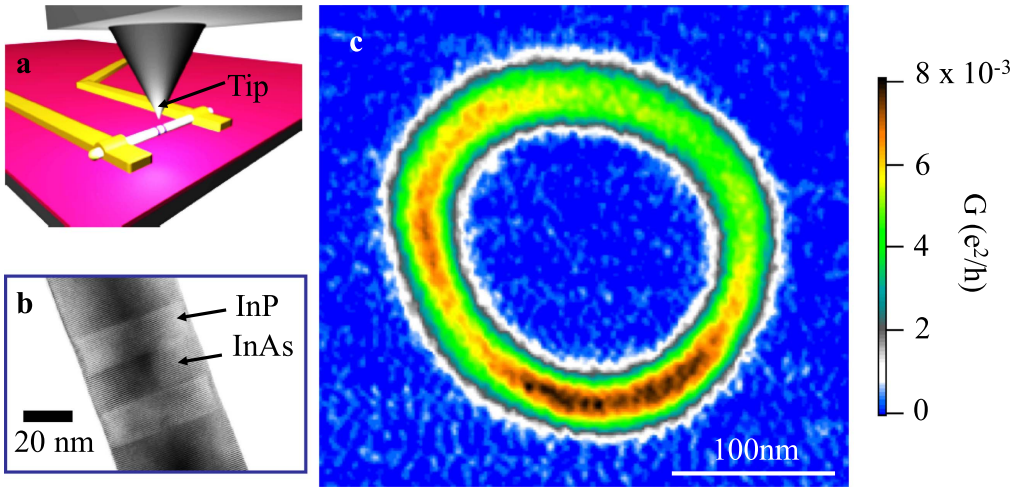

Figure 2. Tuning the charge on an InAs quantum dot in a InP/InAs/InP nanowire. (a) Scanning gate microscope setup (b) TEM image of an InP/InAs/InP quantum dot formed by two InP barriers (c) image of Coulomb blockade conductance versus tip position for the last electron in the quantum dot at temperature 4.2 K. Reprinted with permission from [17] Copyright 2008 by the American Physical Society.

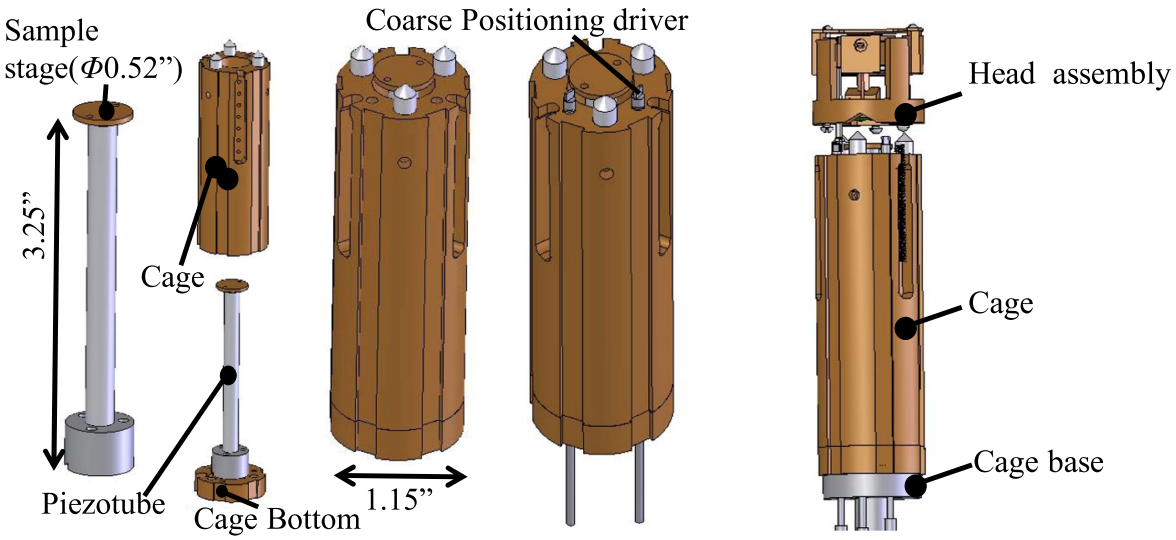

Figure 3. The leftmost figure shows the piezotube with sample stage fixed to a macor insulator on the bottom. Placing the piezotube onto the cage makes the cage assembly shown in the next figure. The rightmost figure shows the coarse positioning devices used to position the SPM cantilever and tip above the sample stage [42].

Experimental apparatus

The cooled SPM used to image electron motion inside graphene devices is described here [42]. The microscope consists of a head assembly containing the tip, and a cage containing the scanning piezotube and the sample holder, shown in figure 3. The sample stage is attached to the top of the piezotube. A typical scan is performed by translating the piezotube horizontally below the tip after setting the SPM tip height above the sample. A coarse positioning system allows the upper head to be moved horizontally relative to the lower head through the vertical motion of two wedges by screws that go to the top of the Dewar.

The cooled SPM uses a piezoresistive cantilever, in which the cantilever deflection and the resulting resistance change is measured by a bridge circuit. High voltages lines that control the piezotube are shielded by stainless steel coaxial cables to reduce the pickup in the sample measurement leads. The SPM electronics include the force-feedback controller to measure the height of the tip above the sample and a digital-to-analog converter to generate the X and Y voltages to perform the scan. The computer integrates SPM sweeps of the sample with conductance data acquisition to create images of electron flow. The SPM lies inside a Liquid-He Dewar that can be operated between 1.5 and 4.2 K.

Measurements of the capacitance between the SPM tip and a sample versus tip voltage provide the opportunity for CV profiling at the nanoscale. We have developed an scanning capacitance microscope to image the tip-to-sample capacitance C_{tip} versus the dc tip voltage, motivated by the work of Ashoori [1–6, 42, 43]. A cooled charge amplifier, shown in figure 4(a) located next to the tip, is used to measure the capacitance. The input noise measured at 4.2 K is 20 nV $Hz^{-1/2}$ and the charge noise is 0.13 e $Hz^{-1/2}$. The

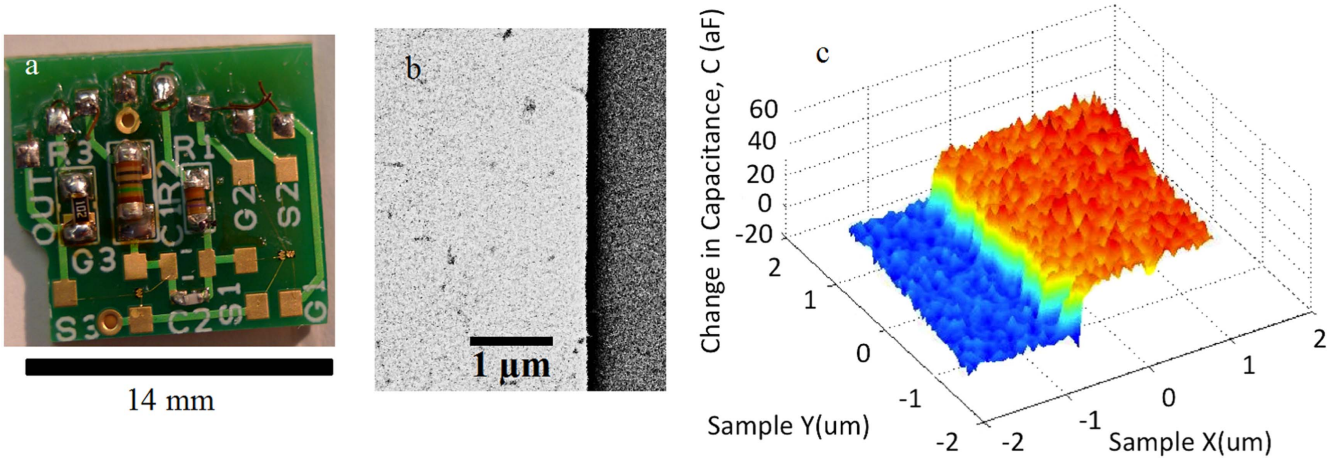

Figure 4. Scanning capacitance microscopy (a) a charge preamplifier mounted next to the SPM cantilever. (b) SEM image of a gold film partially covering a substrate. (c) Capacitance-scan of a sharp tungsten tip above the sample, showing the change in capacitance as the tip is scanned at a height of 20 nm above the edge of the gold film. The FWHM of the capacitance transition is 100 nm [42, 43].

capacitance-profiling setup was tested on a sample consisting of a 15 nm thick gold film on a SiO_x/Si substrate, shown in figure 4(b). The tip to sample capacitance measured as it was scanned across the edge of the gold film, is shown in figure 4(c). A change in capacitance 30 aF was measured as the tip was scanned across the edge of the gold film, with a spatial resolution 100 nm. This tool allows one to do CV profiling of small structures and to probe a quantum dot with just two electrodes, the SPM tip and the sample contact, to facilitate further understanding of low-dimensional nanoscale systems.

Imaging cyclotron orbits in graphene

In this section, we review our recent work imaging cyclotron orbits in graphene in the magnetic focusing regime [41, 42]. Magnetic focusing occurs for electrons traveling from one narrow contact to another in a perpendicular magnetic field B, when the contact spacing L equals the diameter of a cyclotron orbit, as shown in figure 5(a). Orbits leaving the first contact at different angles rejoin at a distance equal to the cyclotron orbit. Additional peaks can occur at higher B when L is an integer multiple of the cyclotron diameter, if the electron orbit skips along the edge [44–46].

To image cyclotron orbits, we used a hBN-graphene-hBN device shown in the inset to figure 6(a) [41, 42]. The device was etched into a Hall-bar geometry with two broad contacts at the ends and two narrow contacts along each side, separated by $L = 2.0\,\mu$m center-to-center. The degree of focusing is measured by the transmission of electrons between the two point contacts, determined by the current I_s in the injecting contact, the voltage V_r measured at the receiving contact, and the change in transresistance $\Delta R_m = V_r/I_s$. With no tip present, the cyclotron orbits on the first magnetic focusing peak join together at the receiving contact. We use our cooled scanning gate microscope to image cyclotron trajectories in graphene as shown in figure 5(b). Cyclotron trajectories deflected from their original

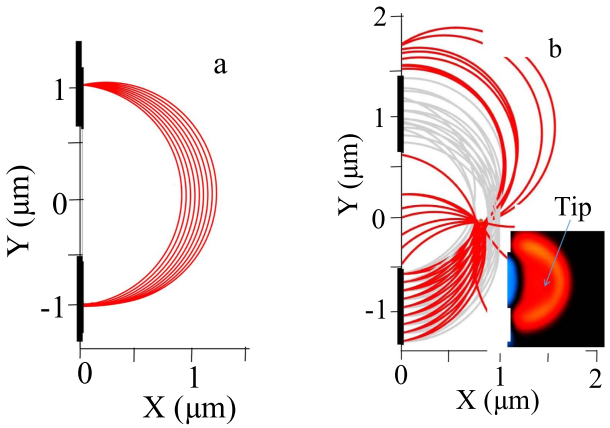

Figure 5. (a) Ray tracing illustration of electron cyclotron trajectories connecting two point contacts in a perpendicular magnetic field. (b) Scattering by the SPM tip for trajectories at $B = 0.130$ T and tip position (0.75, 0) μm. The red trajectories are deflected away from the receiving contact, reducing the transmission. The two narrow contacts are shown as the dark bars on the left of the sample. Reprinted with permission from [41]. Copyright 2016 American Chemical Society.

path reduce the transmission between the two contacts and reduce the transresistance R_m. The inset to figure 5(b) shows a ray tracing simulated image of the transmission change as the tip is raster scanned above the sample—red represents the drop while blue is increase in transmission. This technique allows us to map the cyclotron orbits of electrons in graphene.

Experimentally measured magnetic focusing transmission peaks are shown in figure 6(a), which displays the transresistance R_m as the density n and magnetic field B are scanned at $T = 4.2$ K [41]. The first magnetic focusing peak is clearly shown as the red band of decreased transmission between the two contacts that occurs when the cyclotron diameter is equal to the contact spacing. In addition, one sees a dark band signifying a second magnetic focusing peak at twice the magnetic field. The signal from the second peak is not strong, presumably due to diffuse scattering at the sample edge.

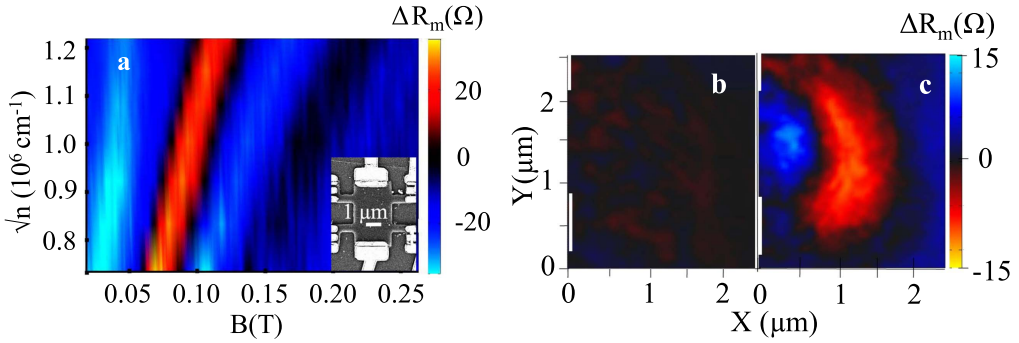

Figure 6. (a) Change in transresistance ΔR_m versus magnetic field B and electron density $n^{1/2}$. Inset shows an SEM image of the hBN-graphene-hBN Hall bar sample. (b) Image of electron flow for $B = 0$; no signal is seen. (c) Image of cyclotron orbits on the first focusing peak in (a). The white bars on the left of (b) and (c) show the location of the narrow contacts. Reprinted with permission from [41]. Copyright 2016 American Chemical Society.

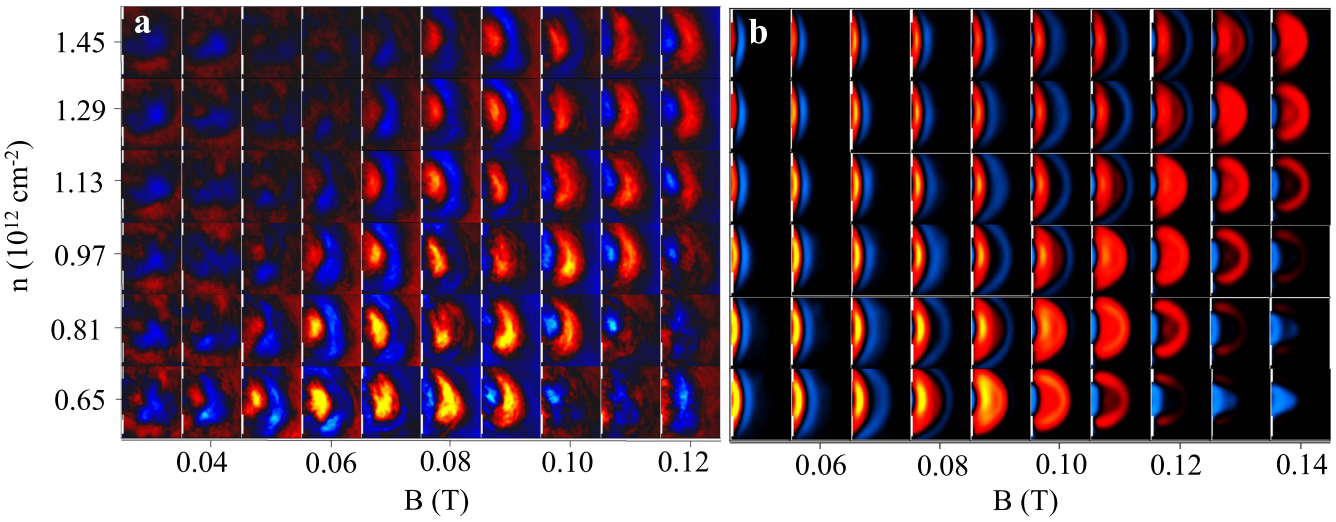

Figure 7. Tiled plots of the transresistance maps as we vary the magnetic field B and electron density n (a) experimental scanning probe microscopy images and (b) ray-tracing simulations. On the first focusing peak in figure 6(a), the cyclotron orbits are clearly shown. Reprinted with permission from [41]. Copyright 2016 American Chemical Society.

Experimental SPM images of electron flow are shown in figures 6(b) and (c) [41]. In the absence of a magnetic field, in figure 6(b), no image is seen as expected, because electrons travel along straight lines that do not connect the two narrow contacts. However, in figure 6(c), when one applies a perpendicular magnetic field B on the first magnetic focusing peak, a clear image of the cyclotron orbit is obtained [41]. The width and shape of the orbit average over electrons that enter the sample at all angles, as illustrated by figure 5. The blue area of increased transmission when the tip is near the edge of the sample, occurs because the tip deflects trajectories away from the diffusely scattering sample edge, as discussed below.

Figures 7(a) and (b) show tiled plots of the experimental SPM images of electron flow and ray-tracing simulations of electron transmission versus B and n over the region of the first magnetic focusing peak, shown in figure 6(a) [41]. Clear visualization of the cyclotron orbit is shown, both in the SPM images and the ray-tracing simulations, which correspond closely. These results demonstrate that the cooled SPM can image ballistic orbits of electron in graphene, opening the way to the development of devices based on ballistic transport.

In addition to the red cyclotron orbits in the experimental images, we also see blue regions of increased transmission between contacts [41]. Figure 8 presents ray tracing simulations that allow us to understand this effect. At low magnetic fields B, (figure 8(a)) the blue region is far from the edge, while at high B, (figure 8(b)) the blue region is close to the edge of the sample. The tip enhances transmission by deflecting electrons into the receiving contact in both cases. At low B in figure 8(a), the cyclotron diameter is large compared with the contact spacing, and the electrons do not make it to the receiving contact. The tip can deflect trajectories to the receiving contact, increasing the transmission. At high B in figure 8(b), the cyclotron orbit is shorter than the contact separation, and electrons diffusively scatter off the edge instead of reaching the second contact. In this case, the tip bounces electrons away from the edge into the receiving contact, increasing the transmission.

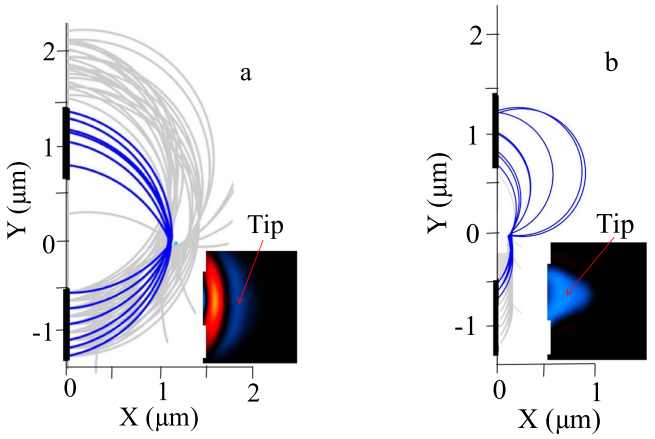

Figure 8. (a) Ray-tracing trajectories for $B = 0.09$ T and tip position (1.0, 0) μm. (d) Ray-tracing trajectories for $B = 0.140$ T and tip position (0.15, 0) μm. The blue regions correspond to an increase in transmission that are a result of the tip deflecting the electron trajectories (a) into the receiving contact or (b) away from the diffusly scattering edge into the drain contact. Reprinted with permission from [41]. Copyright 2016 American Chemical Society.

Conclusion

Imaging electron motion with a cooled SPM provides us with the ability to locally characterize electronic motion in nanoscale structures. The growing number of atomic layer materials, including graphene and transition metal dichalcogenides, such as MoS_2, WSe_2 and black phosphorus, provide opportunities for new types of devices and offer a great opportunity to probe novel physics in low-dimensional systems [47, 48]. For graphene encapsulated by hBN layers, the mean free path can reach several microns. Mapping electron trajectories with SPM promises to be a valuable tool for ballistic device design. Transition metal dichalcogenide materials such as MoS_2, WSe_2, have shorter mean free paths, and transport is typically in the diffusive regime. However, the devices are typically 'hand-made' and our cooled SPM imaging techniques can locally characterize their performance and provide pathways toward better performance by locally probing electron motion at the nanoscale [49]. In addition, SPM imaging can detect quantum dots formed by local minima in the background potential, and it can show the location, diameter, charge state of quantum dots [16], which would be challenging to obtain from transport measurements alone.

The capabilities of cooled scanning gate microscopes are improving. In our group, recent improvements allow coarse positioning of tip at helium temperatures to speed operation [42]. A technique to permit local CV profiling at nanoscale resolution has also been demonstrated [42, 43]. Using the cooled SPM, we were able to image cyclotron orbits of electrons in graphene [41, 42]. The B and n dependence of the cyclotron orbits agree well with simulations of electron trajectories.

Acknowledgments

The SPM imaging research and the ray-tracing simulations were supported by the US DOE Office of Basic Energy Sciences, Materials Sciences and Engineering Division, under grant DE-FG02-07ER46422. Nanofabrication was performed in part at the Center for Nanoscale Systems (CNS) at Harvard University, a member of the NSF National Nanotechnology Coordinated Infrastructure Network (NNCI), supported under NSF award 1541959.

References

[1] Ashoori R C 1996 Electrons in artificial atoms *Nature* **379** 413–9
[2] Tessmer S H, Glicofridis P I, Ashoori R C, Levitov L S and Melloch M R 1998 Subsurface charge accumulation imaging of a quantum Hall liquid *Nature* **392** 51
[3] Finkelstein G, Glicofridis P I, Tessmer S H, Ashoori R C and Melloch M R 2000 Imaging of low compressibility strips in the quantum Hall liquid *Phys. Rev.* B **61** R16323
[4] Steele G 2006 Imaging transport resonances in the quantum Hall effect *PhD Thesis* M.I.T
[5] Steele G A, Ashoori R C, Pfeiffer L N and West K W 2005 Imaging transport resonances in the quantum hall effect *Phys. Rev. Lett.* **95** 136804
[6] Yacoby A, Hess H F, Fulton T A, Pfeiffer L N and West K W 1999 Electrical imaging of the quantum Hall State *Solid State Commun.* **111** 1–13
[7] Topinka M A 2002 Imaging coherent electron wave flow through 2D Electron gas nanostructures *PhD Thesis* Harvard University
[8] Topinka M A, LeRoy B J, Shaw S E J, Heller E J, Westervelt R M, Maranowski K D and Gossard A C 2000 Imaging coherent electron flow from a quantum point contact *Science* **289** 5488
[9] Topinka M A, LeRoy B J, Westervelt R M, Shaw S E J, Fleischmann R, Heller E J, Maranowski K D and Gossard A C 2001 Coherent branched flow in a two-dimensional electron gas *Nature* **410** 6825
[10] LeRoy B J, Topinka M A, Westervelt R M, Maranowski K D and Gossard A C 2002 Imaging electron density in a two-dimensional electron gas *Appl. Phys. Lett.* **80** 23
[11] LeRoy B J, Bleszynski A C, Aidala K E, Westervelt R M, Kalben A, Heller E J, Shaw S E J, Maranowski K D and Gossard A C 2005 Imaging electron interferometer *Phys. Rev. Lett.* **94** 12
[12] Jura M P, Topinka M A, Urban L, Yazdani A, Shtrikman H, Pfeiffer L N, West K W and Goldhaber-Gordon D 2007 Unexpected features of branched through high-mobility two-dimensional electron gases *Nat. Phys.* **3** 12
[13] Aidala K E 2006 Imaging magnetic focusing in a two-dimensional electron gas *PhD Thesis* Harvard University
[14] Aidala K E, Parrott R E, Kramer T, Heller E J, Westervelt R M, Hanson M P and Gossard A C 2007 Imaging magnetic focusing of coherent electron waves *Nat. Phys.* **3** 7
[15] Fallahi P, Bleszynski A C, Westervelt R M, Huang J, Walls J D, Heller E J, Hanson M and Gossard A C 2005 Imaging a single-electron quantum dot *Nano Lett.* **5** 2
[16] Bleszynski-Jayich A C, Zwanenburg F A, Westervelt R M, Roest A L, Bakkers E P A M and Kouwenhoven L P 2007 Scanned probe imaging of quantum dots inside InAs nanowires *Nano Lett.* **7** 2559–62

[17] Bleszynski-Jayich A C, Froberg L E, Bjork M T, Trodahl H J, Samuelson L and Westervelt R M 2008 Imaging a one-electron InAs quantum dot in an InAs/InP nanowire *Phys. Rev.* B **77** 24
[18] Boyd E E, Storm K, Samuelson L and Westervelt R M 2011 Scanning gate imaging of quantum dots in 1D ultra-thin InAs/InP nanowires *Nanotechnology* **22** 18
[19] Gildemeister A E, Ihn T, Schleser R, Ensslin K, Driscoll D C and Gossard A C 2007 Imaging a coupled quantum dot-quantum point contact system *J. Appl. Phys.* **102** 8
[20] Bockrath M, Liang W J, Bozovic D, Hafner J H, Lieber C M, Tinkham M and Park H K 2001 Resonant electron scattering by defects in single-walled carbon nanotubes *Science* **291** 5502
[21] Woodside M T and McEuen P L 2002 Scanned probe imaging of single-electron charge states in nanotube quantum dots *Science* **296** 5570
[22] Martin J, Akerman G, Ulbricht G, Lohmann T, Smet J H, von Klitzing K and Yacoby A 2008 Observation of electron–hole puddles in grapheme using a scanning single-electron transistor *Nat. Phys.* **4** 144–8
[23] Zhang Y, Brar V W, Girit C, Zettl A and Crommie M F 2009 Origin of spatial charge inhomogeneity in graphene *Nat. Phys.* **5** 722–6
[24] Berezovsky J, Borunda M F, Heller E J and Westervelt R M 2010 Imaging coherent transport in graphene : I. Mapping universal conductance *Nanotechnology* **21** 27
[25] Berezovsky J and Westervelt R M 2010 Imaging coherent transport in graphene : II. Probing weak localization *Nanotechnology* **21** 27
[26] Schnez S, Guettinger J, Huefner M, Stampfer C, Ensslin K and Ihn T 2010 Imaging localized states in graphene nanostructures *Phys. Rev.* B **82** 16
[27] Novoselov K S, Geim A K, Morozov S V, Jiang D, Zhang Y, Dubonos S V, Grigorieva I V and Firsov A A 2004 Electric field effect in atomically thin carbon films *Science* **306** 5696
[28] Wallace P R 1947 The band theory of graphite *Phys. Rev.* **71** 622–34
[29] Castro Neto A H, Guinea F, Peres N M R, Novoselov K S and Geim A K 2009 The electronic properties of graphene *Rev. Mod. Phys.* **81** 109–62
[30] Geim A K and Novoselov K S 2007 The rise of graphene *Nat. Mater.* **6** 183–91
[31] Zhang Y, Tan Y W, Stormer H L and Kim P 2005 Experimental observation of the quantum Hall effect and Berry's phase in graphene *Nature* **438** 201–4
[32] Novoselov K S, McCann E, Morozov S V, Fal'ko V I, Katsnelson M I, Zeitler U, Jiang D, Schedin F and Geim A K 2006 Unconventional quantum Hall effect and Berry's phase of 2 pi in bilayer graphene *Nat. Phys.* **2** 177–80
[33] Katsnelson M I, Novoselov K S and Geim A K 2006 Chiral tunneling and the Klein paradox *Nat. Phys.* **2** 620–5
[34] Magda G Z, Jin X, Hagymasi I, Vansco P, Osvath Z, Nemes-Incze N, Hwang C, Biro L P and Tapaszto L 2014 Room-temperature magnetic order on zigzag edge of narrow graphene nanoribbons *Nature* **514** 608–11
[35] Rycerz A, Tworzyd J and Beenakker C W J 2007 Valley filter and valley valve in graphene *Nat. Phys.* **3** 172–5
[36] Morozov S V, Novoselov K S, Katsnelson M I, Schedin F, Ponomarenko L A, Jiang D and Geim A K 2006 Strong suppression of weak localization in graphene *Phys. Rev. Lett.* **97** 016801
[37] Recher P, Trauzettel B, Rycerz A, Blanter Ya M, Beenakker C W J and Morpurgo A F 2007 Aharonov–Bohm effect and broken valley degeneracy in graphene rings *Phys. Rev.* B **76** 235404
[38] Dean C R *et al* 2016 Boron nitride substrates for high-quality graphene electronics *Nat. Nanotechnol.* **5** 722–6
[39] Bolotin K I, Ghahari F, Shulman M D and Kim P 2009 Observation of the fractional quantum Hall effect in graphene *Nature* **462** 196–9
[40] Young A F and Kim P 2009 Quantum interference and Klein tunneling in graphene heterojunctions *Nat. Phys.* **5** 222–6
[41] Bhandari S, Lee G H, Klales A, Watanabe K, Taniguchi T, Heller E, Kim P and Westervelt R M 2016 Imaging cyclotron orbits of electrons in graphene *Nano Lett.* **16** 1690–4
[42] Bhandari S 2015 Imaging electron motion in graphene *PhD Thesis* Harvard University
[43] Bhandari S and Westervelt R M 2014 Low temperature scanning capacitance probe for imaging electron motion *J. Phys.: Conf. Ser.* **568** 3
[44] Sharvin Y V and Fisher L M 1965 Observation of focused electron beams in a metal *J. Exp. Theor. Phys. Lett.* **1** 152
[45] Peierls R 1935 Quelques proprits typiques des corps solides *Ann. Inst. Henri Poincare* **5** 177–222
[46] Taychatanapat T, Watanabe K, Taniguchi T and Jarillo-Herrero P 2013 Electrically tunable transverse magnetic focusing in graphene *Nat. Phys.* **9** 225–9
[47] Braun M, Chirolli L and Burkard G 2008 Signature of chirality in scanning-probe imaging of charge flow in graphene *Phys. Rev.* B **77** 115433
[48] Chang C, Zhao W, Kim D Y, Zhang H, Assaf B A, Heiman D, Zhang S, Liu C, Chan M H W and Moodera J S 2015 High-precision realization of robust quantum anomalous Hall state in a hard ferromagnetic topological insulator *Nat. Mater.* **14** 472–7
[49] Bhandari S, Wang K, Watanabe K, Taniguchi T, Kim P and Westervelt R M 2016 Imaging electron motion in a few layer MoS_2 device arxiv:1608.02250